Proceedings Paper:
Okada, T., Azakli, Y. and Morley, N.A. (2026) Effect of praseodymium addition on magnetostriction of Fe-Al alloys. In: 2026 IEEE International Magnetic Conference - Short Papers (INTERMAG Short Papers). 2026 IEEE International Magnetic Conference - Short Papers (INTERMAG Short Papers), 13-17 Apr 2026, Manchester, U.K.. Institute of Electrical and Electronics Engineers (IEEE). ISBN: 9798331557638.

https://doi.org/10.1109/intermagshortpapers68882.2026.11595973

Effect of Praseodymium Addition on Magnetostriction of Fe–Al Alloys

Taku Okada, Yunus Azakli and Nicola A. Morley, *Senior Member, IEEE*

School of Chemical, Materials and Biological Engineering, University of Sheffield, Sheffield, S1 3JD, United Kingdom

Magnetostriction is essential for developing superior magnetic materials for vibration energy harvesting. In this study, rare-earth elements were added to Fe–Al melt-spun ribbons to increase magnetostriction. The crystal structure of the $Fe_{81}Al_{19}$ ribbon was estimated to be predominantly an A2-(Fe, Al) disordered phase based on XRD data and Rietveld analysis. In the $Fe_{75}Al_{18.75}Pr_{6.25}$ and $Fe_{75}Al_{18.75}Tb_{6.25}$ ribbons, not only the A2-(Fe, Al) phase but also the Pr_2Fe_{17} phase and Tb_2Fe_{17} phase were confirmed, respectively. The saturation magnetostrictive strain parallel to the magnetic field direction in $Fe_{81}Al_{19}$ ribbon shows 30 ppm. This value is consistent with the theoretical value of a {110} plane-oriented sample. While the parallel magnetostrictive strain at 0.35 T in the $Fe_{75}Al_{18.75}Tb_{6.25}$ ribbon is 15 ppm, the $Fe_{75}Al_{18.75}Pr_{6.25}$ ribbon is 26 ppm. This result suggests that the enhancement of magnetostriction by Pr addition may be greater compared to Tb. Consequently, adding Pr into Fe–Al alloys is an effective approach to improve magnetostrictive properties.

***Index Terms*— Magnetostriction, Fe–Al alloy, Rare earth elements, Praseodymium**

I. Introduction

The strain change associated with the direction of magnetisation is known as the magnetostrictive effect. This effect can be used for various applications such as actuators, sensors, and vibration energy harvesting [1]. A magnetostrictive material has a large magnetostrictive strain, which is determined by the material-specific magnetostrictive constants λ_{100} and λ_{111} in the <100> and <111> directions, respectively.

Various studies have proposed magnetostrictive materials, such as Tb–Dy–Fe compounds [2], Fe–Ga alloys [3], Fe–Al alloys [4], and Fe–Co alloys [5]. Tb–Dy–Fe compounds have exhibited a giant magnetostriction (e.g. $Tb_{0.27}Dy_{0.73}Fe_{1.95}$ has a λ_{100} of 100 ppm and λ_{111} of 1600 ppm [2]). However, they are brittle and expensive because of the heavy rare-earth elements Dy and Tb. Particularly, for vibration energy harvesting that applies stress to the magnetostrictive materials, alloys with high ductility are preferable [6], [7]. Fe–Ga alloys have shown a large magnetostriction (e.g. Fe–18.7 at.% Ga alloy has exhibited λ_{100} of 263 ppm [3]) and ductility. Al in Group 13, same as Ga, also has increased the magnetostriction from Fe (λ_{100} of 20.7 ppm and λ_{111} of –21.2 ppm [8]), exhibiting λ_{100} of 103 ppm and λ_{111} of 1 ppm at 19.5 at.% Al [4]. Although Fe–Al alloys are inferior to Fe–Ga alloys in terms of magnetostriction, they have a cost advantage.

Among the numerous third elements added to Fe–Al alloys or Fe–Ga alloys, rare-earth elements, particularly Tb, have demonstrated significant effects in enhancing magnetostriction [9], [10], [11], [12]. This improvement is due to the crystal orientation and an increase in the magnetostrictive constants. The increase in the magnetostrictive constants appears to be attributed to several factors: the disk-shaped distribution of Tb's 4*f* orbitals, strong spin-orbit coupling, and promoting the formation of a tetragonal modified-$D0_3$ phase in the A2 phase[12]. However, Tb belongs to the heavy rare-earth elements, leading to increased costs (e.g. average price of Terbium oxide is $1,010/kg in 2025 [13]). Therefore, this study focused on Pr, a light rare-earth element that is less expensive (e.g. average price of Praseodymium oxide is $74/kg in 2025 [13]). Like Tb, Pr possesses disk-shaped 4*f* orbitals. Moreover, the addition of the element with a larger atomic radius to Fe results in an increase in the lattice constant, leading to an enhancement of the magnetic moment [14]. Due to lanthanide contraction, the atomic radius of Pr (1.828 Å) is larger than that of Tb (1.782 Å) [15].

Most previous studies have focused on additions of 1 at.% or less. However, we considered adding several at.% may be effective for improving the material's intrinsic magnetostrictive constants, rather than for improving orientation. Therefore, in this study, the atomic ratio of the rare earth element added to the Fe–Al alloy was set at 6.25 at.%. Because heavy atoms such as rare-earth elements are difficult to dissolve in Fe, rapid cooling via the melt spinning method was employed. This study aims to clarify the magnetostrictive properties of melt-spun ribbons made from Fe–Al alloys with Pr addition. For comparison, Fe–Al–Tb alloys were also investigated.

II. Experimental

The precursor ingots of $Fe_{81}Al_{19}$, $Fe_{75}Al_{18.75}Pr_{6.25}$, and $Fe_{75}Al_{18.75}Tb_{6.25}$ were arc-melted from the elements with a minimum purity of 99.9% using an Arcast Arc 200 unit at least three times. These ingots were subsequently remelted and melt-spun into ribbons using an Arcast SC100 melt spinner.

The obtained ribbon was subjected to X-ray diffraction (XRD) data acquisition using the STOE STADI P, which is a pure Mo Kα_1 source in transmission geometry. Rietveld analysis was performed to extract detailed crystallographic information from the XRD data. In the Rietveld analysis, a split pseudo-Voigt profile function was employed, and fitting was

Manuscript received April 1, 2015; revised May 15, 2015 and June 1, 2015; accepted July 1, 2015. Date of publication July 10, 2015; date of current version July 31, 2015. (Dates will be inserted by IEEE; "published" is the date the accepted preprint is posted on IEEE Xplore®; "current version" is the date the typeset version is posted on Xplore®). Corresponding author: F. A. Author (e-mail: f.author@nist.gov). If some authors contributed equally, write here, "F. A. Author and S. B. Author contributed equally." IEEE TRANSACTIONS ON MAGNETICS discourages courtesy authorship; please use the Acknowledgment section to thank your colleagues for routine contributions.

Color versions of one or more of the figures in this paper are available online at http://ieeexplore.ieee.org.

Digital Object Identifier (inserted by IEEE).

carried out using the least squares method. Crystallographic Information File (CIF) used as the crystallographic model was obtained from The Materials Project [16], [17]. Magnetic properties were obtained using the SQUID magnetometer MPMS3 from Quantum Design at 300 K and fields up to 1 T.

Magnetostrictive strain was measured using the strain gauge method. This method is a technique in which a strain gauge containing a resistive wire is attached to the sample, and the change in resistance caused by the sample's deformation is converted into a strain value. As shown in Fig. 1 (a), the strain gauge was attached by sandwiching it between the ribbons. This configuration suppresses the bending strain induced by the applied magnetic field in the thin ribbon sample. As shown in Fig. 1 (b), the magnetic field H was applied to the sample. The magnetostrictive strains ε^{m}, parallel to the H direction ($\theta = 0°$) and perpendicular to the H direction ($\theta = 90°$) were measured by rotating the sample holder. A dummy gauge was employed to compensate for changes in the strain gauge's resistance due to temperature and magnetic-field variations. The change in the strain gauge's resistance, corresponding to the strain of the sample, was detected by a bridge circuit.

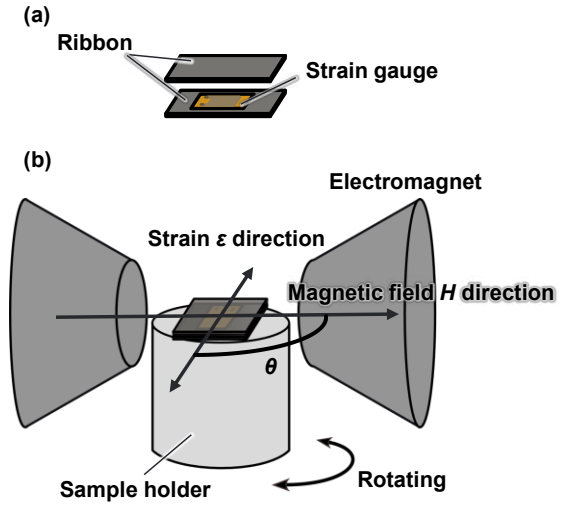

Fig. 1. Schematic illustration of (a) the sample and (b) the magnetostrictive measurement system.

III. Results and Discussion

The results of XRD and Rietveld analysis for the $Fe_{81}Al_{19}$ ribbon are shown in the Fig. 2. The lower part of the figure indicates the peak positions for the $D0_3$-Fe_3Al order phase and A2-(Fe, Al) disorder phase. For the $Fe_{81}Al_{19}$ ribbon, superlattice peaks of the $D0_3$-Fe_3Al phase were not observed. Furthermore, to evaluate the degree of ordering, the order parameter was incorporated into the Rietveld analysis. The order parameter ranges from 0 to 1, where 0 indicates random and 1 indicates perfect order. In this analysis, the order parameter was 0.15, suggesting the phase is predominantly A2 disordered. The lattice parameter a was determined to be 2.89 Å, which is in good agreement with previous studies (2.8970 Å for quenched $Fe_{81.2}Al_{18.8}$ [18]).

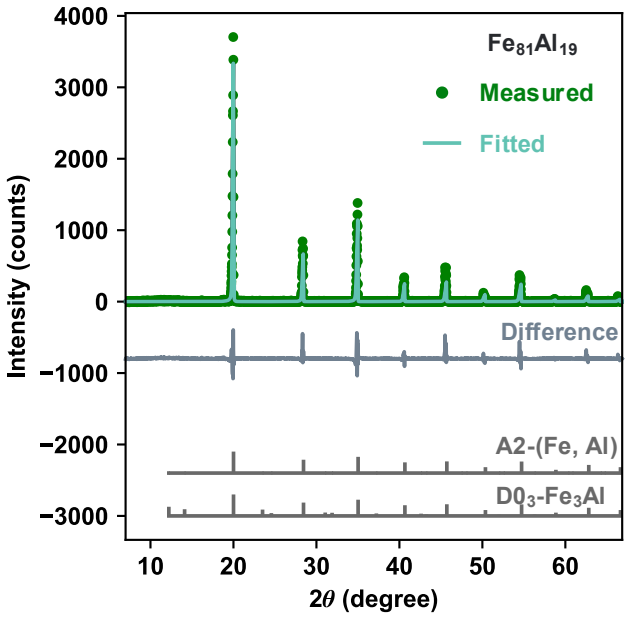

Fig. 2. XRD and Rietveld analysis results of $Fe_{81}Al_{19}$ ribbon using Mo Kα_1 source. Measured and fitted intensities are represented by the circle symbol and the solid line, respectively. The difference between the two intensities is plotted below them on the same scale as above.

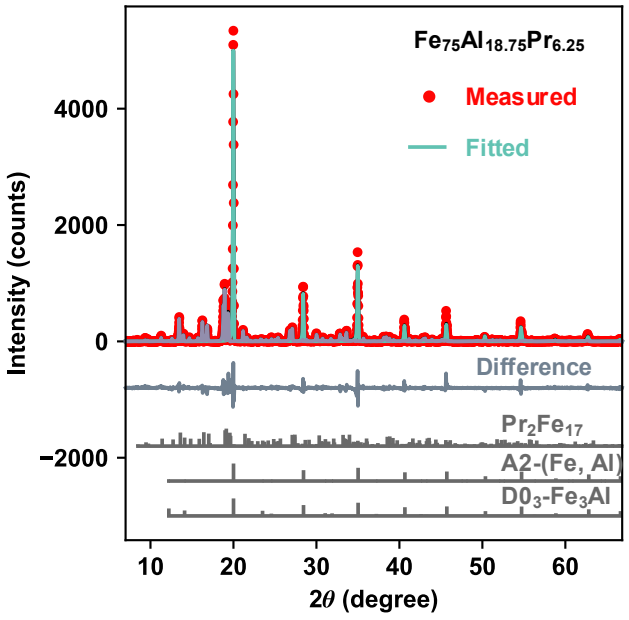

Fig. 3. XRD and Rietveld analysis results of $Fe_{75}Al_{18.75}Pr_{6.25}$ ribbon using Mo Kα_1 source. Measured and fitted intensities are represented by the circle symbol and the solid line, respectively. The difference between the two intensities is plotted below them on the same scale as above.

Fig. 3 shows the XRD and Rietveld analysis results for the $Fe_{75}Al_{18.75}Pr_{6.25}$ ribbon. For the $Fe_{75}Al_{18.75}Pr_{6.25}$ ribbon, peaks corresponding to the A2-(Fe, Al) phase and the Pr_2Fe_{17} phase are observed. This result is consistent with the phases predicted from the Fe–Al–Pr phase diagram [19]. Rietveld analysis estimated the weight fractions of the A2-(Fe, Al) phase and $Pr_2(Fe, Al)_{17}$ phase to be 0.83:0.17. The lattice parameter a, for

the A2-(Fe, Al) phase was estimated as 2.89 Å, while the lattice parameters a and c for the $Pr_2(Fe, Al)_{17}$ phase were estimated as 8.69 Å and 12.7 Å, respectively. Fig. 4 shows the XRD and Rietveld analysis results for the $Fe_{75}Al_{18.75}Tb_{6.25}$ ribbon. Rare earth elements tend to have similar valence electron configurations, resulting in comparable chemical properties. In the $Fe_{75}Al_{18.75}Tb_{6.25}$ ribbon, peaks corresponding to the A2-(Fe, Al) phase and the Tb_2Fe_{17} phase are identifiable. The weight fractions of the A2-(Fe, Al) phase and the $Tb_2(Fe, Al)_{17}$ phase were estimated to be 0.88:0.12, yielding results similar to the $Fe_{75}Al_{18.75}Pr_{6.25}$ ribbon. In the estimation of lattice parameters, a for the A2-(Fe, Al) phase was 2.89 Å, while a and c for the $Tb_2(Fe, Al)_{17}$ phase were 8.54 Å and 12.3 Å, respectively. No change in the lattice parameter of the A2-(Fe, Al) phase was observed in all samples. This result suggests that Pr and Tb did not dissolve into the A2 phase. The smaller lattice parameters of the $Tb_2(Fe, Al)_{17}$ phase compared to the $Pr_2(Fe, Al)_{17}$ phase are likely due to lanthanide contraction [15].

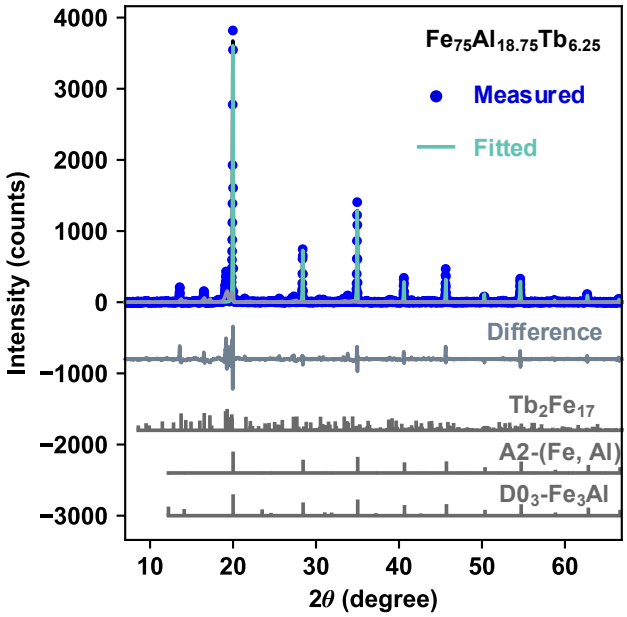

Fig. 4. XRD and Rietveld analysis results of $Fe_{75}Al_{18.75}Tb_{6.25}$ ribbon using Mo Kα_1 source. Measured and fitted intensities are represented by the circle symbol and the solid line, respectively. The difference between the two intensities is plotted below them on the same scale as above.

Fig. 5 shows the magnetic field μ_0H dependence of the magnetisation μ_0M obtained by the SQUID-VSM. The μ_0M (T) was calculated from the magnetic moment (emu) using the density (cm^3/g) obtained from XRD and the sample mass (g). The magnetisation at μ_0H = 1 T for $Fe_{81}Al_{19}$, $Fe_{75}Al_{18.75}Pr_{6.25}$, and $Fe_{75}Al_{18.75}Tb_{6.25}$ ribbons are 1.54 T, 0.94 T, and 0.20 T, respectively. The saturation magnetisation of $Fe_{81}Al_{19}$ was almost consistent with previous studies (1.56 T for $Fe_{81.5}Al_{18.5}$ [20]). These results indicate that the precipitation of the Tb_2Fe_{17} phase significantly reduces the magnetisation at μ_0H = 1 T, whereas the precipitation of the Pr_2Fe_{17} phase causes a smaller reduction in magnetisation at μ_0H = 1 T. This difference arises because light rare-earth elements couple ferromagnetically with Fe, whereas heavy rare-earth elements couple antiferromagnetically with Fe [21]. Furthermore, the coercivities of $Fe_{81}Al_{19}$, $Fe_{75}Al_{18.75}Pr_{6.25}$, and $Fe_{75}Al_{18.75}Tb_{6.25}$ ribbons are 3.4 mT, 2.5 mT, and 20 mT, respectively. Thus, Tb_2Fe_{17} exhibits larger magnetic anisotropy compared to Pr_2Fe_{17}. In other words, Pr can be expected to act as an element that can be substituted into Fe–Al alloys with relatively little loss of saturation magnetisation and soft magnetic properties compared to Tb.

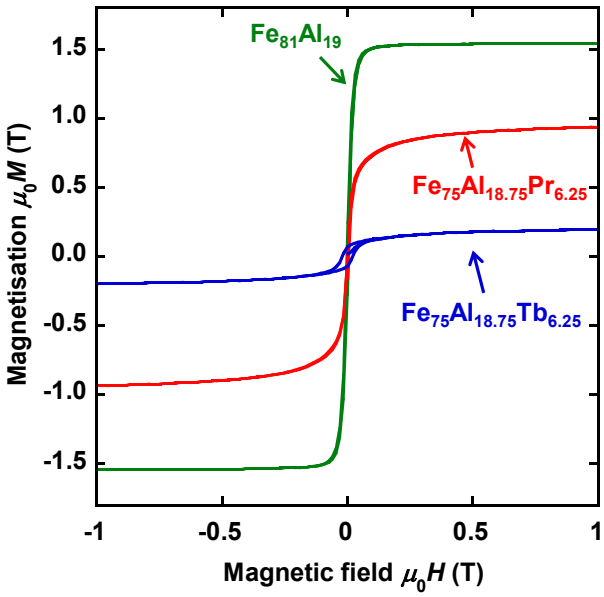

Fig. 5. Magnetic field μ_0H dependence of the magnetisation μ_0M of $Fe_{81}Al_{19}$, $Fe_{75}Al_{18.75}Pr_{6.25}$, and $Fe_{75}Al_{18.75}Tb_{6.25}$ ribbons.

Fig. 6 shows the magnetic field dependence of the magnetostrictive strain of $Fe_{81}Al_{19}$, $Fe_{75}Al_{18.75}Pr_{6.25}$, and $Fe_{75}Al_{18.75}Tb_{6.25}$. The magnetostrictive strains parallel to the magnetic field direction $\varepsilon_{\parallel}^{m}$ of all samples exhibit positive values, while the perpendicular strains $\varepsilon_{\perp}^{m}$ exhibit negative values. The saturation values of $\varepsilon_{\parallel}^{m}$ and $\varepsilon_{\perp}^{m}$ in $Fe_{81}Al_{19}$ are 30 ppm and 15 ppm respectively, exhibiting a 2:1 ratio. This result suggests that the crystallographic orientation within the ribbon plane is isotropic. Furthermore, as Fe–Al alloys tend to grow preferentially along the <110> direction during solidification [22], it is anticipated that the ribbon plane is oriented along the {110} plane. Magnetostrictive strain ε^m can be expressed using the direction cosines of the magnetisation $\boldsymbol{\alpha} = (\alpha_1, \alpha_2, \alpha_3)$ and the direction cosine of the strain $\boldsymbol{\beta} = (\beta_1, \beta_2, \beta_3)$ relative to the crystal orientation, as follows [8]:

$$\varepsilon^m = (3/2)\lambda_{100}(\alpha_1^2\beta_1^2 + \alpha_2^2\beta_2^2 + \alpha_3^2\beta_3^2 - 1/3) + 3\lambda_{111}(\alpha_1\alpha_2\beta_1\beta_2 + \alpha_2\alpha_3\beta_2\beta_3 + \alpha_3\alpha_1\beta_3\beta_1). \quad (1)$$

When the crystal orientation within the ribbon plane is isotropic and the {110} plane is oriented perpendicular to the ribbon plane, the angle φ between the [100] direction within the ribbon plane and magnetisation direction (or strain direction) satisfies $\boldsymbol{\alpha} = \boldsymbol{\beta} = \left(\cos\varphi, \sqrt{2}/2 \sin\varphi, \sqrt{2}/2 \sin\varphi\right)$. From (1), the strain dependent on φ is given by the following:

$$\varepsilon^m_{\{110\}} = (3/2)\lambda_{100}(\cos^4\varphi + (1/2)\sin^4\varphi - 1/3) + 3\lambda_{111}(\cos^2\varphi \sin^2\varphi + (1/4)\sin^4\varphi). \quad (2)$$

Taking the average over all directions in (2) yields the strain for {110} plane-oriented sample, as follows: $\langle\varepsilon^m_{\{110\}}\rangle = (11/32)\lambda_{100} + (21/32)\lambda_{111}$. From λ_{100} of 80.1 ppm and λ_{111} of 2.0 ppm in the quenched Fe–19.5 at.% Al alloy [4], $\langle\varepsilon^m_{\{110\}}\rangle$ is 28.8 ppm, consistent with the experimental $\varepsilon^m_{\parallel}$ value.

Compared to $Fe_{81}Al_{19}$, the magnetostrictive curves of $Fe_{75}Al_{18.75}Pr_{6.25}$ and $Fe_{75}Al_{18.75}Tb_{6.25}$ show an obviously shallow slope, indicating increased magnetic anisotropy. XRD data revealed that $Pr_2(Fe, Al)_{17}$ phase and $Tb_2(Fe, Al)_{17}$ phase precipitated in the $Fe_{75}Al_{18.75}Pr_{6.25}$ ribbon and $Fe_{75}Al_{18.75}Tb_{6.25}$ ribbon, respectively. This precipitation increased the magnetic anisotropy of the $Fe_{75}Al_{18.75}Pr_{6.25}$ ribbon and $Fe_{75}Al_{18.75}Tb_{6.25}$ ribbon, thereby preventing the saturation of the magnetostrictive strain. It has been reported that the magnetostrictive strain of Pr_2Fe_{17} does not saturate even at 2 T [23].

In this experiment, as the magnetostrictive strain of the $Fe_{75}Al_{18.75}Pr_{6.25}$ ribbon does not reach saturation, a comparison of saturation values is not possible. In the future, magnetostriction measurements under higher magnetic fields will be required to obtain the saturation value. However, no improvement in magnetostriction was observed by adding Pr to the Fe–Al alloy. This result can be explained by the extreme difficulty of dissolving Pr in the A2-(Fe, Al) phase. Furthermore, it has been reported that the magnetostriction of Pr_2Fe_{17} is 360 ppm at 53 K but only 32 ppm at 300 K [23]; this result suggests that the $Pr_2(Fe, Al)_{17}$ phase does not contribute to the improvement in the magnetostriction of Fe–Al alloys at room temperature.

However, the $\varepsilon^m_{\parallel}$ value of $Fe_{75}Al_{18.75}Pr_{6.25}$ at μ_0H = 0.35 T is 26 ppm, which is larger than that of $Fe_{75}Al_{18.75}Tb_{6.25}$ (15 ppm). The origin of magnetostriction derives from the anisotropy of the electronic orbitals [14]. The 4*f* electron orbitals of Pr and Tb are significantly distorted into a disk shape, contributing to the large magnetic anisotropy and magnetostriction. Furthermore, since the magnetic moment of Fe is primarily attributed to the spin magnetic moment, linking the orbital anisotropy to the spin magnetic moment requires a strong spin-orbit coupling (SOC), which couples the spin and orbital magnetic moments, and a large orbital magnetic moment. The SOC constant of Tb^{3+} (1707 cm^{-1}), which has a higher atomic number, is greater than that of Pr^{3+} (751.7 cm^{-1}) [24]. Consequently, it is inferred that the $Fe_{75}Al_{18.75}Tb_{6.25}$ ribbon exhibited larger coercivity and magnetic anisotropy in the magnetostrictive curve than the $Fe_{75}Al_{18.75}Pr_{6.25}$ ribbon. However, other key factors are expected to affect magnetostriction. In fact, experimental results show that, although the $Fe_{75}Al_{18.75}Tb_{6.25}$ ribbon exhibits obviously larger anisotropy than the $Fe_{75}Al_{18.75}Pr_{6.25}$ ribbon, its magnetostriction is smaller. In addition to anisotropic electron orbitals and the SOC, other key factors are proposed, such as the large orbital magnetic moment and the strong Coulomb interactions with neighbouring atoms due to the large 4*f* orbital radius. The orbital angular momentum of Pr^{3+} is 5, larger than 3 for Tb^{3+} [8]. Furthermore, in accordance with the lanthanide contraction, the 4*f* orbital radius in Pr is larger than that in Tb [15]. For the reasons outlined above, it can be explained that Pr-added Fe–Al alloys exhibit a larger magnetostrictive strain than Tb-added Fe–Al alloys.

The comparison between $Fe_{75}Al_{18.75}Pr_{6.25}$ ribbon and $Fe_{75}Al_{18.75}Tb_{6.25}$ ribbon is considered to represent the intrinsic influence of Pr and Tb on magnetostrictive properties. Moreover, it is expected that the magnetostriction of Fe–Al alloys can be significantly improved if Pr is successfully dissolved in the A2-(Fe, Al) phase in greater quantities by increasing quenching rates or adding other elements. Therefore, the enhancement of magnetostrictive properties through Pr addition has the potential to surpass that of Tb.

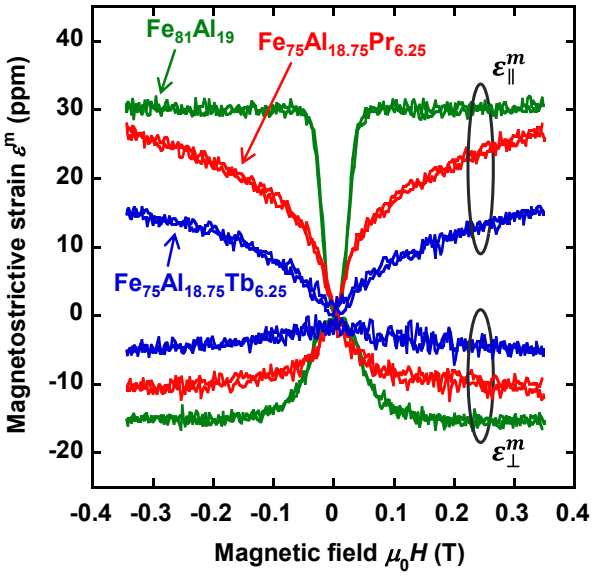

Fig. 6. Magnetic field dependence of the magnetostrictive strain of $Fe_{81}Al_{19}$, $Fe_{75}Al_{18.75}Pr_{6.25}$, and $Fe_{75}Al_{18.75}Tb_{6.25}$.

IV. Conclusion

This study examined the crystal structures, magnetisation characteristics, and magnetostrictive properties of Fe–Al alloys with added Pr and Tb. The crystal structure of the $Fe_{81}Al_{19}$ ribbon was identified to be mainly an A2 disordered phase. In the $Fe_{75}Al_{18.75}Pr_{6.25}$ and $Fe_{75}Al_{18.75}Tb_{6.25}$ ribbons, $Pr_2(Fe, Al)_{17}$ and $Tb_2(Fe, Al)_{17}$ phases precipitated alongside the A2-(Fe, Al) phase. The weight fractions of the $Pr_2(Fe, Al)_{17}$ phase in the $Fe_{75}Al_{18.75}Pr_{6.25}$ ribbon and the $Tb_2(Fe, Al)_{17}$ phase in the $Fe_{75}Al_{18.75}Tb_{6.25}$ ribbon relative to the A2-(Fe, Al) phase were 17% and 12%, respectively. From the magnetisation curves measured by SQUID-VSM, the saturation magnetisation of the $Fe_{81}Al_{19}$, $Fe_{75}Al_{18.75}Pr_{6.25}$, and $Fe_{75}Al_{18.75}Tb_{6.25}$ ribbons was 1.54 T, 0.94 T, and 0.20 T, respectively. These results show that the precipitation of the $Tb_2(Fe, Al)_{17}$ phase considerably reduces the saturation magnetisation. Furthermore, it was found that precipitation of the $Pr_2(Fe, Al)_{17}$ phase causes a smaller reduction in saturation magnetisation than that caused by $Tb_2(Fe, Al)_{17}$. Magnetostriction measurements revealed that the magnetostrictive strain parallel to the magnetic field in the

$Fe_{81}Al_{19}$ ribbons reached a saturation value of 30 ppm. This value matched the theoretical value for {110} plane-oriented samples. The magnetostrictive strain parallel to the magnetic field in the $Fe_{75}Al_{18.75}Tb_{6.25}$ ribbon at a magnetic field of 0.35 T was 15 ppm, while in the $Fe_{75}Al_{18.75}Pr_{6.25}$ ribbon, it was 26 ppm. These results suggest that the electronic structure of Pr effectively contributes to the enhancement of magnetostrictive properties. Therefore, the addition of Pr to Fe–Al alloys is expected to yield new magnetostrictive materials.

ACKNOWLEDGEMENT

This work was supported by the Japan Society for the Promotion of Science (JSPS) Overseas Research Fellowships.

REFERENCES

[1] Z. Deng and M. J. Dapino, 'Review of magnetostrictive vibration energy harvesters', *Smart Mater. Struct.*, vol. 26, no. 10, p. 103001, Oct. 2017, doi: 10.1088/1361-665X/aa8347.

[2] J. P. Teter, A. E. Clark, and O. D. McMasters, 'Anisotropic magnetostriction in Tb0.27Dy0.73Fe1.95', *J. Appl. Phys.*, vol. 61, no. 8, pp. 3787–3789, Apr. 1987, doi: 10.1063/1.338646.

[3] A. E. Clark *et al.*, 'Extraordinary magnetoelasticity and lattice softening in bcc Fe-Ga alloys', *J. Appl. Phys.*, vol. 93, no. 10, pp. 8621–8623, May 2003, doi: 10.1063/1.1540130.

[4] R. C. Hall, 'Single Crystal Anisotropy and Magnetostriction Constants of Several Ferromagnetic Materials Including Alloys of NiFe, SiFe, AlFe, CoNi, and CoFe', *J. Appl. Phys.*, vol. 30, no. 6, pp. 816–819, Jun. 1959, doi: 10.1063/1.1735247.

[5] T. Okada, S. Fujieda, S. Seino, and T. Nakagawa, 'Evaluation of Magnetic Flux Density Change for Vibration Energy Harvesting: Comparison Between Direct and Indirect Measurements', *IEEE Trans. Magn.*, vol. 59, no. 11, pp. 1–5, Nov. 2023, doi: 10.1109/TMAG.2023.3283960.

[6] T. Okada *et al.*, 'Vibration Power Generation Property of U-Shaped Unimorph Device Using Grain-Oriented Electrical Steel', *Mater. Trans.*, vol. 62, no. 12, pp. 1798–1801, Dec. 2021, doi: 10.2320/matertrans.MT-M2021079.

[7] T. Sugiyama *et al.*, 'Application of Various Materials With Negative Saturation Magnetostriction to Vibration Power Generation', *IEEE Trans. Magn.*, vol. 59, no. 11, pp. 1–6, Nov. 2023, doi: 10.1109/TMAG.2023.3285254.

[8] S. Chikazumi and C. D. Graham, *Physics of ferromagnetism*, 2. ed., 1. publ. in paperback. in International series of monographs on physics, no. 94. Oxford: Oxford Univ. Press, 2009.

[9] Y. Han, H. Wang, T. Zhang, Y. He, and C. Jiang, 'Giant magnetostriction in nanoheterogeneous Fe-Al alloys', *Appl. Phys. Lett.*, vol. 112, no. 8, p. 082402, 2018, doi: 10.1063/1.5023273.

[10] R. Wang, X. Tian, Z. Yao, X. Zhao, and H. Hao, 'Influence of rare earth element terbium doping on microstructure and magnetostrictive properties of Fe81Al19 alloy', *J. Rare Earths*, vol. 40, no. 3, pp. 451–456, Mar. 2022, doi: 10.1016/j.jre.2020.12.009.

[11] J. S. Uribe-Chavira, G. Herrera-Pérez, C. R. Santillán-Rodríguez, R. J. Sáenz-Hernández, J. A. Matutes-Aquino, and M. C. Grijalva-Castillo, 'X-ray diffraction analysis by Rietveld refinement of FeAl alloys doped with terbium and its correlation with magnetostriction', *J. Rare Earths*, vol. 41, no. 8, pp. 1217–1224, Aug. 2023, doi: 10.1016/j.jre.2022.07.006.

[12] Y. He *et al.*, 'Giant heterogeneous magnetostriction in Fe–Ga alloys: Effect of trace element doping', *Acta Mater.*, vol. 109, pp. 177–186, May 2016, doi: 10.1016/j.actamat.2016.02.056.

[13] National Minerals Information Center, 'Mineral Commodity Summaries 2026 Data Release'. U.S. Geological Survey. doi: 10.5066/P1WKQ63T.

[14] R. M. Bozorth, *Ferromagnetism*. New York: IEEE Press, 1993.

[15] T. Moller, *The chemistry of the lanthanides*. in Pergamon texts in inorganic chemistry, no. volume 26. Oxford: Pergamon Press, 1975.

[16] A. Jain, S. P. Ong, G. Hautier, and others, 'Commentary: The Materials Project: A materials genome approach to accelerating materials innovation', *APL Mater.*, vol. 1, no. 1, p. 011002, Jul. 2013, doi: 10.1063/1.4812323.

[17] M. K. Horton *et al.*, 'Accelerated data-driven materials science with the Materials Project', *Nat. Mater.*, vol. 24, no. 10, pp. 1522–1532, Oct. 2025, doi: 10.1038/s41563-025-02272-0.

[18] A. Taylor and R. M. Jones, 'Constitution and magnetic properties of iron-rich iron-aluminum alloys', *Journal of Physics and Chemistry of Solids*, vol. 6, no. 1, pp. 16–37, Jul. 1958, doi: 10.1016/0022-3697(58)90213-0.

[19] R. Freccero, L. Arrighi, G. Cacciamani, and P. Riani, 'The 500 °C Isothermal Section of the Al-Fe-Pr Ternary System', *J. Phase Equilib. Diffus.*, vol. 45, no. 3, pp. 596–611, Jun. 2024, doi: 10.1007/s11669-024-01117-8.

[20] J. B. Restorff, M. Wun-Fogle, K. B. Hathaway, A. E. Clark, T. A. Lograsso, and G. Petculescu, 'Tetragonal magnetostriction and magnetoelastic coupling in Fe-Al, Fe-Ga, Fe-Ge, Fe-Si, Fe-Ga-Al, and Fe-Ga-Ge alloys', *J. Appl. Phys.*, vol. 111, no. 2, p. 023905, Jan. 2012, doi: 10.1063/1.3674318.

[21] R. C. O'Handley, *Modern magnetic materials: principles and applications*. New York: Wiley-Interscience, 2000.

[22] Z. Dai *et al.*, 'Enhancing magnetostriction in FeAl alloys via crystal growth orientation tuning by a trace amount of Pt doping', *Journal of Materials Research and Technology*, vol. 33, pp. 3376–3383, Nov. 2024, doi: 10.1016/j.jmrt.2024.10.038.

[23] A. E. Clark, S. F. Cheng, J. P. Teter, M. Wun-Fogle, M. Q. Huang, and Y. Zheng, 'Effect of nitrogenation on the magnetostriction of Y2Fe17, Pr2Fe17 and Nd2Fe17', *Journal of Magnetism and Magnetic Materials*, vol. 104–107, pp. 1433–1434, Feb. 1992, doi: 10.1016/0304-8853(92)90651-4.

[24] W. T. Carnall, G. L. Goodman, K. Rajnak, and R. S. Rana, 'A systematic analysis of the spectra of the lanthanides doped into single crystal LaF3', *J. Chem. Phys.*, vol. 90, no. 7, pp. 3443–3457, Apr. 1989, doi: 10.1063/1.455853.